OCA-B/Pou2af1 is sufficient to promote CD4$^+$ T cell memory and prospectively identifies memory precursors

Wenxiang Sun[1,2,†,¶], Erik P. Hughes[1,2,†], Heejoo Kim[1,2,†,Ψ], Jelena Perovanovic[1,2,§], Krystal R. Charley[1,2], Junhong Du[1,2], Andrea Ibarra[1,2], J. Scott Hale[1], Matthew A. Williams[1,2], Dean Tantin[1,2,3,*]

[1]Department of Pathology, University of Utah School of Medicine, Salt Lake City, UT 84112, U.S.A.
[2]Huntsman Cancer Institute, University of Utah School of Medicine, Salt Lake City, UT 84112, U.S.A.
[3]Lead contact

[*]Correspondence author: Dean Tantin
Email: dean.tantin@path.utah.edu

Author contributions:
M.A.W., D.T. designed research; W.S., E.P.H., H.K., K.R.C., J.D., A.I. performed research; J.S.H., M.A.W. contributed research tools; W.S., H.K., J.P., K.R.C. analyzed data; W.S., E.P.H., H.K., J.P., K.R.C., J.D., A.I., J.S.H., M.A.W., D.T. wrote the manuscript.

Competing interest statement: The authors declare that they have no competing interests.
Classification: Immunology
Keywords: Immunological memory | CD4 T cells | Pou2af1/OCA-B

[†]Equal contributors
[¶]Current address: Sumitomo Pharma Oncology, 3900 N. Traverse Mountain Blvd., Suite 100, Lehi, Utah 84043
[Ψ]Current address: Janssen Research & Development, LLC., Neuroimmunology Drug Discovery, 3210 Merryfield Row, San Diego, CA 92121.
[§]Current address: Recursion Pharmaceuticals, 41 400 W, Salt Lake City, UT 84101

Words in abstract: 162
Words in MS (excluding references): 6,471

Abstract

The molecular mechanisms leading to the establishment of immunological memory are inadequately understood, limiting the development of effective vaccines and durable anti-tumor immune therapies. Here we show that ectopic OCA-B expression is sufficient to drive T cells towards a memory fate, while having minimal effects on primary antiviral effector response. At primary effector response, short lived effector T cell compartments are expanded but show increased expression of *Gadd45b* and *Socs2*, while memory precursor effector cell clusters show increased expression of *Bcl2*, *Il7r* and *Tcf7* on a per cell basis, consistent with increased memory potential. Using an OCA-B mCherry reporter mouse line, we observe high OCA-B expression in $CD4^+$ T_{CM} cells. We show that during viral infection, endogenously elevated OCA-B expression prospectively identifies memory precursor cells with increased survival capability and memory recall potential. Cumulatively, the results demonstrate that OCA-B is both necessary and sufficient to promote CD4 T cell memory in vivo and can be used to prospectively identify memory precursor cells.

Significance

$CD4^+$ T cell memory is incompletely defined and memory progenitors are difficult to identify. Here, we show that expression of the OCA-B transcription coactivator in $CD4^+$ T cells is necessary and sufficient to drive productive memory. Using a novel mCherry reporter mouse strain, we show that OCA-B expression can be used to enrich responding effector cells with elevated potential to form memory. The results show that OCA-B expression in T cells is sufficient to promote $CD4^+$ memory formation and marks memory precursor cells.

Introduction

The ability to respond robustly to secondary antigen exposures (immune memory) is a defining feature of the adaptive immune system and forms the physiologic basis for vaccination (1). Immune memory can also drive autoimmune and antitumor responses (2-5). Strategies that promote memory have the potential to improve both vaccine efficacy and tumor immunotherapy. Central memory T cells (T_{CM}), which home to secondary lymphoid organs, are particularly long lived and demonstrate high proliferative capacity upon stimulation.

Multiple transcription factors and epigenetic regulators are known to modulate formation or function of T_{CM}, including Blimp1 (6-8), Suv39h1 (9), T-bet (10, 11), Foxo1 (12, 13), Bcl6 (14, 15), Eomes (16) and TCF1 (17). Many of these factors regulate memory less clearly in $CD4^+$ compared to $CD8^+$ T cells. In $CD4^+$ T cells, the lymphocyte-restricted transcriptional coregulator OCA-B (also known as OBF-1 and Pou2af1) is induced upon T cell antigen stimulation (18, 19). Germline OCA-B deletion results in normal primary T cell responses to LCMV, but attenuates $CD4^+$ memory T cell formation and recall response. Elevated *Ocab* (*Pou2af1*) mRNA levels are seen in $CD4^+CD25^{lo}$ early effector cells that are enriched for memory potential (20). OCA-B is also associated with autoimmunity (21-24).

Here, we show that OCA-B deletion in T cells selectively reduces memory responses. We show that ectopic OCA-B expression does not alter effector cell numbers at peak T cell response to LCMV, but is sufficient to expand the memory recall effector pool at the expense of empty vector (EV)-transduced controls. The effect becomes progressively stronger at later timepoints. mRNA expression profiling of effector cells ectopically expressing OCA-B reveals gene expression changes associated with effector and memory properties, signaling and homing. These include global increases in *Socs2* and *Gadd45b*, expansion of short-lived terminal effector T cell populations, and increases in *Tcf7* and *Il7r* in specific memory precursor populations. Using an OCA-B reporter mouse, we show that elevated levels of endogenous OCA-B in effector T cells during the primary response prospectively identifies $CD4^+$ T effector cells with enhanced survival and expansion capability following viral rechallenge.

Results and Discussion

OCA-B in T cells is required for robust $CD4^+$ T cells memory recall responses

We used a conditional *Ocab* (*Pou2af1*) mouse allele crossed to a CD4-Cre driver, which efficiently deletes OCA-B in T cells (24), to study effects of T cell-specific OCA-B loss. We infected $Ocab^{fl/fl}$;CD4-Cre and control $Ocab^{fl/fl}$ mice with $LCMV^{Arm}$ and measured specific T cell responses using $I\text{-}A^b/gp_{66-77}$ tetramer staining. No significant differences in the frequency of positive cells were observed at 8 days post-primary infection (dpi, Fig. S1*A*). Rechallenging these mice with *Listeria monocytogenes* expressing the LCMV glycoprotein epitope (Lm-gp61) (25) elicited a trending but nonsignificant

91 decrease in the frequency of CD4$^+$ I-A^b/gp$_{66–77}$$^+$ CD4$^+$ T cells undergoing memory recall response in
92 *Ocab*$^{fl/fl}$;CD4-Cre mice (Fig. S1*A*, D40+7). The responding cells showed little change in IL-2/IFNγ
93 double-producing CD4$^+$ T cells, but a significant decrease in IFNγ single-producers (Fig. S1*B*, *C*). The
94 same cells showed minimal changes in ICOS, PD-1, Ly6C or CD62L expression (Fig. S1*D*). These
95 results indicate that infection of T cell-conditional OCA-B knockout mice with LCMV results in
96 deficiencies in memory recall response IFNγ expression.
97 The relatively small reductions in frequencies of tetramer$^+$ CD4$^+$ T cells at recall response may
98 reflect selection for a small percentage of cells escaping OCA-B deletion. This selection can be
99 circumvented using bone marrow chimeras in which conditional deficient or control cells are competed
100 against wild-type T cells in the same mice. We generated bone marrow radiation chimeras in which
101 wild-type donors were co-engrafted with congenically-marked *Ocab*$^{fl/fl}$;CD4-Cre or control *Ocab*$^{fl/fl}$ cells
102 in the same recipients. After 8 weeks to allow engraftment, recipient mice were infected with LCMV.
103 The ratio of antigen-reactive *Ocab*$^{fl/fl}$ control effector CD4$^+$ T cells to wild-type competitor was close to
104 1:1 at 8 dpi. OCA-B deficient (*Ocab*$^{fl/fl}$;CD4-Cre) cells were slightly reduced relative to wild-type
105 competitor (Fig. S1*E*). To investigate the effects of T cell-specific OCA-B loss on memory recall
106 responses, we rechallenged mice with Lm-gp61. Following rechallenge, the control to wild-type cell
107 ratio remained close to 1:1 at both primary and memory recall response, while wild-type competitor
108 cells were greatly increased at the expense of OCA-B deficient cells specifically at recall. (>8-fold, Fig.
109 S1*E*, *F*). These findings indicate that, similar to T cell-conditional Oct1 deficiency and global OCA-B
110 deficiency (26), T cell-conditional OCA-B deficiency in bone marrow chimeras results in severe and
111 selective deficiencies in CD4$^+$ T cell memory recall responses.
112
113 **Ectopic OCA-B expression is sufficient to enhance CD4$^+$ T cell memory responses in vivo**
114 We transduced Thy1.1$^+$ SMARTA TCR transgenic donor CD4$^+$ T cells with a retroviral vector
115 expressing mouse OCA-B. In parallel, Ly5.1$^+$ (CD45.1$^+$) control SMARTA cells were transduced with
116 EV. SMARTA mice express a transgenic TCR recognizing an immunodominant LCMV glycoprotein
117 (GP$_{61–80}$) CD4$^+$ epitope (27). GFP$^+$ Thy1.1$^+$ SMARTA expressing OCA-B and GFP$^+$ Ly5.1 SMARTA
118 (EV) cells were sorted, mixed 1:1 and adoptively co-transferred into Thy1.2$^+$Ly5.2$^+$ recipients (Fig.
119 1*A*). Efficient OCA-B expression was confirmed using fibroblasts (Fig. 1*B*). After transfer, recipient
120 mice were infected with LCMV and the cell populations were detected by flow cytometry using GFP
121 expressed from MSCV and congenic markers from the donor T cells. The host T cells mounted
122 normal responses to LCMV, allowing SMARTA cells to be monitored in the context of a normal host
123 response. At 8 dpi, effector EV and OCA-B transduced cells expanded equivalently, maintaining the
124 same ratio in both spleen and peripheral blood (Fig. 1*C* and D). Another group of mice were infected
125 with LCMV and allowed to clear the virus and form memory. Recall responses were induced by re-

126 challenge using Lm-gp61. At peak T cell response to rechallenge (52+7 and 110+7 dpi), ~50-fold
127 more OCA-B overexpressing SMARTA cells were present (Fig. 1*C* and *D*). Ratios of percentages
128 from multiple mice are quantified in Fig. 1*E*. These results indicate that OCA-B expression enhances
129 the ability of $CD4^+$ T cells to induce memory responses.
130 At 8 dpi, GFP^+ SMARTA effector T cells were uniformly $CD44^{hi}CD62L^{lo}$ with few changes
131 induced by ectopic OCA-B expression (Fig. 1*F*). ICOS and PD-1 levels were slightly diminished by
132 OCA-B overexpression. Ly6C was not significantly altered (Fig. 1*F* and *G*). To investigate if ectopic
133 OCA-B expression induces gene expression changes in effector cells that promote later memory
134 formation, we profiled gene expression using splenic SMARTA T cells at 8 dpi. $CD4^+$ cells were first
135 isolated by magnetic isolation, then $Ly5.1^+/5.2^+$ and GFP^+ cells were further isolated by FACS. We
136 identified ~600 down-regulated genes and ~200 up-regulated genes (Table S1). Unsupervised
137 hierarchical clustering identified differentially expressed gene clusters (Fig. 2*A*). Down-regulated
138 genes included *Sell*, which encodes CD62L, and genes specific to alternative $CD4^+$ lineages, such as
139 *Bcl6* and *Foxp3*. The top up-regulated gene, *Pou2af1*, encodes OCA-B, providing a quality control.
140 Other up-regulated genes were associated with effector activity (*Tbx21*, *Zeb2*), exhaustion
141 (*Ikzf2*/*Helios*) and attenuation of T cell signaling and proliferation (*Socs2*, *Gadd45b*). *Gadd45b*
142 promotes autoimmune disease and anti-tumor immune responses (28-31). Example genome tracks
143 are shown in Fig. 2*B*. Gene ontology (GO) analysis of the up-regulated genes identified terms
144 associated with H3K9me3 regulation. Down-regulated genes by contrast were strongly associated
145 with H3K27me3 in $CD4^+$ and $CD8^+$ memory T cells (Fig. 2*C*). ChIP-X Enrichment Analysis (ChEA)
146 (32) identifies Tp53 and Smc3 as factors that also regulate the gene set induced by OCA-B ectopic
147 expression (Fig. 2*D*). p53 and SMC3 may therefore also control expression of these genes alongside
148 OCA-B, or could themselves be controlled by OCA-B to mediate gene induction via an indirect
149 mechanism. Sets of significant Molecular Function, Epigenomic Roadmap and ChEA GO terms are
150 shown in Table S2. These changes may be sufficient to confer potential increased memory formation,
151 as small advantages compounded over time can result in the large observed effects.
152 Two other genes associated with T cell survival and memory formation, *Il7r* and *Tcf7*, were
153 decreased in bulk RNA-seq. *Il7r* encodes a cytokine receptor critical for T cell survival, while Tcf7
154 encodes TCF1 which promotes naïve, Tfh and memory T cell transcriptional programs (11, 17).
155 Effector $CD4^+$ T cell populations are heterogeneous, with memory progenitor cells comprising a small
156 proportion of the effector T cell population (11, 20, 33). In bulk RNA-seq, icreased expression of
157 genes that promote memory in rare memory progenitors may therefore be obscured by decreases in
158 terminal effector cells. To test this, we performed single-cell RNA-sequencing (scRNA-seq) at D8
159 post-LCMV infection. Uniform manifold approximation and projection (UMAP) using EV-transduced
160 cells revealed a variety of populations (Fig. 3*A*, Table S3). Clusters 1 and 4 were enriched for genes
161 such as *Ccr7*, *Bcl2*, *Slamf6* and *Tcf7* (both clusters), *Tox* (cluster 1), and *Cxcr5*, *Il7r*, *Icos* and *Cd69*

162 (cluster 4, Table S3). These clusters likely contain memory precursors. Clusters 0, 2 and 6 by contrast
163 were enriched in *Ccl5*, *Ifng* and *Tbx21*, respectively (Table S3), and likely comprise terminal effectors.
164 Cluster 5 was enriched for genes encoding histones, cyclin-dependent kinases and proliferating cell
165 nuclear antigen (PCNA) and likely represent proliferating effectors.
166 OCA-B-transduction resulted in more uniform clustering with fewer and more tightly spaced
167 clusters identified using the same parameters (Fig. 3*B*). Cluster 0 effector cells were marked by *Zeb2*,
168 *Klrg1* and *Tbx21* (Table S3). Clusters 1 and 2 were also associated with effector activity. OCA-B
169 transduced cluster 3 was associated with effector/memory progenitor activity similar to EV-transduced
170 clusters 1 and 4 (Fig. 3*C*). Although there were proportionately fewer of these cells compared to the
171 EV-transduced clusters 1 and 4, multiple memory-associated genes were increased on a per cell
172 basis. *Tcf7* was increased by >4-fold in OCA-B cluster 3 relative to other clusters, but only 2-fold in EV
173 clusters 1 and 4 (Table S3). *Slamf6* was increased by >3-fold in OCA-B cluster 3, but <2.5-fold in EV
174 clusters 1 and 4. *Bcl2* and *Il7r* were similarly more strongly expressed relative to the other clusters in
175 OCA-B- compared to EV-transduced cells. Additionally, *Foxo1* was not over-represented in either
176 memory-associated EV cluster but was enriched in OCA-B cluster 3, while *Ikzf2*, which has been
177 associated with $CD4^+$ T cell exhaustion (34), was not enriched in cluster 3 but was enriched in the
178 equivalent EV-transduced clusters (Table S3). Simultaneously, OCA-B-transduced clusters showed
179 broad increases in the expression of *Socs2*, which encodes an attenuator of T cell signal transduction,
180 and *Gadd45b*, which promotes growth arrest (Fig. 3*C*). These findings suggest that OCA-B
181 transduced cells in cluster 3 are qualitatively superior to their EV-transduced counterparts at forming
182 memory.
183 Clustering EV- and OCA-B-transduced cells together allows the relative proportions of cells
184 with common gene expression features to be determined. Again, specific clusters were enriched for
185 effector cells (Fig. 3*D*, clusters 0, 1, 2, 4, 6), proliferating effector cells (5) and effector cells with
186 memory progenitor potential (3). Feature plots for key genes are shown in Fig. 3*E*. In the OCA-B-
187 transduced condition, cluster 3 contained proportionately fewer cells but showed elevated expression
188 of genes such as *Il7r* and *Gadd45b* on a per cell basis (Fig. 3*F*). These findings identify changes in
189 gene expression and effector T cell populations consistent with increased memory potential.
190
191 **OCA-B knock-in reporter mice label $CD4^+$ memory T cell populations**
192 To monitor OCA-B expression in viable cells, we knocked 3 mCherry reporter cassettes preceded by
193 P2A elements into the mouse *Pou2af1* (*Ocab*) locus. The resulting reporter allele contained the
194 mCherry cassettes inserted immediately before the stop codon and the 3' UTR (Fig. 4*A*). A successful
195 hemizygous knock-in founder and a homozygote generated by intercrossing the progeny were
196 confirmed by PCR (Fig. S2*A*). Hemizygous and homozygous reporter mice retained normal OCA-B
197 protein expression (Fig. S2*B*). We used flow cytometry to identify peripheral blood mCherry-

198 expressing cells from hemizygous and homozygous reporter mice and wild-type controls. OCA-B was
199 readily detectable in B cells (Fig. S2*C*, *D*). Peripheral T cell expression was weaker, forming a
200 shoulder in hemizygous reporters, but a discrete peak in homozygotes (Fig. S2*C*, *D*). We therefore
201 used heterozygous mice to characterize B cell populations, and homozygous mice to study T cells.
202 Robust mCherry expression could be detected in the bone marrow, peritoneal cavity, spleen
203 and lymph nodes of specific pathogen-free hemizygous reporter mice. Total thymocytes by contrast
204 expressed little OCA-B (Fig. S2*E*). We used IgM and B220 to discriminate developing, immature and
205 recirculating bone marrow B cells. OCA-B expression was readily detected in developing, immature
206 and recirculating B cell populations compared to wild-type controls (Fig. S2*F*). Expression was nearly
207 uniform in the different populations, except for a small population of immature B cells that lacked
208 OCA-B expression. Peritoneal B-1 and B-2 B cells were also homogeneous, with stronger expression
209 in B-2 relative to B-1 cells (Fig. S2*G*). Splenic B cells can be partitioned into transitional and mature
210 populations based on CD93 (AA4.1) staining. T1/2/3 subsets stratified by CD23 and IgM uniformly
211 expressed OCA-B (Fig. S2*H*). CD21 and CD23 expression divides mature splenic B cells into
212 marginal zone (MZ), follicular and non-follicular populations, and all three populations expressed
213 OCA-B strongly (Fig. S2*I*). Expression was largely uniform, but there was a significant population of
214 newly formed $CD21^{lo}CD23^{lo}$ B cells expressing no OCA-B. The nature and significance of these cells
215 is unknown. These results document strong reporter activity in B cell populations, with the highest
216 level of activity in MZ and B-1 B cells. MZ B cells are largely absent in OCA-B knockout mice (35).
217 These results indicate that the OCA-B reporter robustly labels B cells.
218 Gating out B cells, approximately 5% of thymocytes from unchallenged, specific pathogen-free
219 homozygous reporter mice expressed OCA-B (Fig. S2*J*). mCherry expression could be identified in
220 CD4/CD8 double-negative (DN), DP and SP compartments, with the highest amounts in DN and CD8
221 SP cells (Fig. S2*K*). In the spleen, the relative abundance of $CD4^+$ and $CD8^+$ T cells was unaltered by
222 the homozygous reporter allele (Fig. 4*B*). Splenic $CD4^+$ T cells express mCherry at ~50-fold lower
223 levels compared to B cells and with a wider range of expression (Fig. 4*C*). Peripheral blood T cell
224 mCherry levels varied over a similar range (not shown).
225 We used CD62L and CD44 to stratify resting splenic $CD4^+$ and $CD8^+$ cells into naïve,
226 activated/effector and central memory compartments. Reporter activity could be detected in
227 approximately 7% of naïve ($CD62L^{hi}CD44^{lo}$) cells (Fig. 4*D*). The nature of these cells (e.g., Tregs,
228 Tscm, recent thymic emigrants) is unknown. Progressively larger fractions of early activated
229 ($CD62L^{lo}CD44^{lo}$), activated ($CD62L^{lo}CD44^{hi}$) and T_{CM} ($CD62L^{hi}CD44^{hi}$) cells expressed mCherry (Fig.
230 4*D*). Naïve $CD8^+$ T cells showed comparatively higher expression levels, but decreased expression in
231 the activated state and similar expression in T_{CM} cells (Fig. 4*E*). Therefore, within the $CD4^+$ T cell
232 compartment, increased OCA-B expression as measured by mCherry fluorescence progressively
233 labels greater fractions of naïve, activated and central memory $CD4^+$ cells.

234

235 **Elevated OCA-B expression prospectively enriches memory precursor CD4$^+$ T cells**

236 To assess OCA-B responses during infection, memory formation and rechallenge, we infected
237 reporter mice with LCMV and used MHC tetramers to identify splenic T cells recognizing
238 immunodominant LCMV epitopes. Prior to infection, >90% of cells were naïve phenotype, with 13.7%
239 of these mCherry$^+$. ~50% of activated CD44^{hi} cells expressed mCherry (Fig. S3*A*, D0). Similarly, 50%
240 of 8 dpi effector cells expressed mCherry regardless of tetramer status (Fig. S3*B*, D8). After LCMV
241 clearance, memory timepoint mice showed higher percentages of mCherry (D43, 61.6%), though with
242 lower expression per cell. Rechallenge with Lm-gp61 to generate CD4$^+$ T cell antigen-specific recall
243 responses reduced mCherry positivity compared to resting memory, and high-affinity tetramer$^+$ cells
244 declining from >60% to <10% mCherry (Fig. S3*A*, D42+7). In contrast, a higher percentage of CD8$^+$
245 reporter T cells expressed mCherry prior to infection. Higher percentages of tetramer$^+$ mCherry$^+$ were
246 also present at 5 dpi, but by 8 dpi (peak T cell response) mCherry was reduced (Fig. S3*B*). Antigen
247 specific memory CD8$^+$ T cells also showed reduced mCherry levels relative to CD4$^+$ (Fig. S3*B*). We
248 did not collect data on CD8$^+$ rechallenge because Lm-gp61 does not express the CD8-dominant
249 epitope recognized by H2-D^b LCMV tetramers.

250 To determine if OCA-B expression in responding CD4$^+$ T cells is associated with increased
251 memory potential, we crossed the reporter allele to a SMARTA TCR transgenic background to fix the
252 TCR specificity and to the Ly5.1 congenic marker to track engrafted cells. We transferred cells into
253 recipients, infected with LCMV, isolated mCherry^{hi} and mCherry^{lo} cells at 8 dpi, transferred large
254 numbers of cells (8×10^5) into naïve secondary recipient mice, and isolated splenic CD4$^+$ T cells to
255 assess contraction (Fig. 5*A*). More cells were recovered from mice engrafted with mCherry^{hi} cells,
256 indicating that these cells contracted less than mCherry^{lo} controls (Fig. 5*B*, *C*). Interestingly the cells
257 that did survive showed similar mCherry fluorescence (Fig. 5*D*). These findings indicate that effector
258 CD4$^+$ cells expressing higher OCA-B undergo less cell death when transferred into naïve animals.

259 To test the ability of the cells expressing OCA-B to mount antigen recall responses, we
260 similarly transferred congenically marked SMARTA cells into recipient mice and infected with LCMV,
261 but isolated mCherry^{hi} and mCherry^{lo} cells at 43 dpi. 4×10^4 of memory SMARTA cells were transferred
262 into naïve hosts, which were challenged with LCMV and analyzed at 7 dpi (Fig. 5*E*). mCherry^{hi}
263 SMARTA cells mounted better recall responses compared to mCherry^{lo} (Fig. 5*F*, *G*) though again with
264 little difference in mCherry fluorescence intensity (Fig. 5*H*). This result indicates a plasticity in OCA-B
265 expression whereby expression normalizes following antigen re-encounter.

266 In mice, OCA-B expression can be detected, varying over a 10-fold range, in responding cells
267 as early as one day after infection with lymphocytic choriomeningitis virus (LCMV) (26). Memory
268 progenitor cells characterized by low CD25 expression can be identified as early as early as 3 dpi (14,

269 20). We transferred SMARTA homozygous OCA-B mCherry reporter T cells into congenic recipients,
270 infected with LCMV, and collected spleens at 3 dpi to study mCherry and CD25 levels (Fig. 5*I*). A
271 large fraction of responding $CD25^{lo}$ SMARTA cells expressed mCherry (Fig. 5*J*). SMARTA cells from
272 the same mouse expressing low levels of CD25 also expressed high levels of TCF1, as expected
273 (20). mCherry and TCF1 were not compared as cell fixation quenches mCherry, however we were
274 able to directly compare CD25 and OCA-B. $CD25^{hi}$ cells expressed a range of OCA-B, while $CD25^{lo}$
275 cells were highly enriched for $mCherry^{hi}$ cells (Fig. 5*K*, *L*). These findings show that high OCA-B
276 expression can be used as a method to prospectively mark live $CD4^+$ memory precursor effector T
277 cells with augmented capacity to form central memory. Identifying transcriptional regulators that define
278 the memory precursor effector $CD4^+$ T cells will promote advances in understanding the formation of
279 CD4 T cell memory. Cumulatively, this study indicates that OCA-B expression within $CD4^+$ T cells is
280 both necessary for, and sufficient to promote, the emergence of T_{CM}.

281 **Materials and methods**

282 **Mice**

283 All mice used in this study were on the C57BL6/J strain background. All mouse experiments were
284 approved by the University of Utah Institutional Animal Care and Use Committee (protocol 00001553).
285 *Pou2af1* (*Ocab*) conditional (floxed) mice were described previously (24). *Pou2af1*-3×mCherry
286 reporter knock-in mice were generated on a C57BL/6N background (Biocytogen), but were
287 backcrossed >5 times to C57BL/6J prior to generation of data herein.

288

289 **LCMV and *Listeria* infection**

290 LCMV Armstrong 53b ($LCMV^{Arm}$) (36) was grown in BHK cells and titered using Vero cells (27). For
291 primary infection, 8-to 12-week-old $Ocab^{fl/fl}$ or $Ocab^{fl/fl}$;CD4-Cre mice were inoculated i.p. with 2×10^5
292 plaque-forming units (PFU) of LCMV intraperitoneally.
293 For heterologous rechallenge with *Listeria monocytogenes* expressing LCMV glycoprotein 61-80 (Lm-
294 gp61) (25), bacteria were grown in log phase in BHI media, and concentrations were calculated using
295 OD at 600 nm (OD of $1=1\times10^9$ CFU/mL). Mice were rechallenged intravenously with 2×10^5 colony
296 forming units (CFU) of Lm-gp61 the indicated number of days after primary infection as published
297 (37).

298

299 **Bone marrow radiation chimeras**

300 Radiation chimeras were generated as published (38). Briefly, male Ly5.1 C57BL/6J mice were used
301 as recipients. Mice received a split dose of 900 Rad (2×450 RAD, spaced 1 hr apart), and were
302 engrafted one day later with 1 million mixed donor bone marrow cells. Competitor bone marrow cells
303 from Ly5.2/Thy1.1 but otherwise wild-type mice, and experimental cells from Ly5.2/Thy1.2 $Ocab^{fl/fl}$ or
304 littermate $Ocab^{fl/fl}$;CD4-Cre mice, were isolated from femurs and tibias of donor mice. After red blood
305 cell lysis, $CD3^+$ cells were depleted using biotinylated anti-CD3 antibodies (eBioScience) and anti-
306 biotin magnetic MicroBeads (Miltentyi Biotech) according to the manufacturer's instructions. CD3-
307 depeleted bone marrow cells were mixed 1:1 and injected retro-orbitally. The chimeras were rested
308 for 8 weeks to allow engraftment, after which mice were infected as above. Virus-reactive cells were
309 identified by $LCMVgp_{66–77}$:I-Ab tetramer staining.

310

311 **pMSCV-IRES-GFP-OCA-B vector generation**

312 Wild-type *Ocab* cDNA was amplified from the plasmid pcDNA3.1-OCA-B (39) (a gift from Robert
313 Roeder, Rockefeller University) by PCR and cloned into the pMSCV-IRES-GFP (pMIGR1) retroviral
314 vector (a gift from Ryan O'Connell, University of Utah). Primers used for amplification were mOcab-F-
315 XhoI, 5'CTCGAGCTGTCTGCTTCAAAGAGAAAAGGCAAC; mOcab-R-*Eco*RI, 5'

316 GAATTCCTAAAAGCCCTCCACGGAGAGGGT. The PCR product was gel purified, digested with
317 *Eco*RI and *Xho*I, and inserted into a similarly digested pMIGR1 backbone using T4 DNA ligase to
318 generate pMIGR1-OCA-B. All constructs were validated by resequencing.
319
320 **$CD4^+$ T cell isolation and stimulation**
321 Naïve splenic $CD4^+$ T cells were isolated and simulated as described previously (40). Briefly, spleens
322 were dissociated by grinding and passing through a 70 μm nylon strainer. Red blood cells were lysed
323 by ACK lysis buffer (150 mM NH_4Cl, 10 mM $KHCO_3$, 0.1 mM EDTA). Cells were isolated from mice
324 using a naïve $CD4^+$ T cell isolation kit (Miltenyi), and stimulated in culture using 10 μg/mL plate-bound
325 anti-CD3ϵ and 2 μg/mL anti-CD28 antibodies (eBioscience).
326
327 **Ectopic OCA-B expression in $CD4^+$ T cells**
328 T cells from Ly5.1 SMARTA and Thy1.1 SMARTA mice were purified using a $CD4^+$ T cell isolation kit
329 (Miltenyi). Cells were placed into RPMI 1640 medium supplemented with 10% fetal bovine serum, 50
330 U/mL penicillin, 50 μg/mL streptomycin, 2 mM L-glutamine, 1 mM sodium pyruvate, 1× MEM
331 nonessential amino acids, 55 μM 2-mercaptoethanol, and 20 IU/mL recombinant human IL-2. All
332 components were from ThermoFisher with the exception of IL-2, which was supplied by R&D
333 Systems. Cells were simultaneously transduced with pMIGR retroviruses packaged in 239T cells, with
334 or without expressed mouse OCA-B cDNA, using spin infection. For spin infection, cells were
335 centrifuged with 293T retroviral supernatant at 1000×*g* for 2 hr at 37°C in the presence of 4 μg/mL
336 polybrene (Sigma). On the following day, transduced GFP^+ cells were isolated by fluorescent-
337 activated cell sorting. 2×10^4 pMIGR1- and pMIGR1-OCA-B-transduced cells were combined and co-
338 transferred into wild-type (Ly5.2/Thy1.2) C57BL6/J mice. Chimeric mice were infected with LCMV and
339 re-challenged with Lm-gp61 as described above.
340
341 **Flow cytometry**
342 Spleens were dissociated and passed through a 70 μm nylon strainer. Red blood cells were lysed by
343 ACK lysis buffer (150 mM NH_4Cl, 10 mM $KHCO_3$, 0.1 mM EDTA). For intracellular staining, cell
344 suspensions in RPMI supplemented with 10% fetal bovine serum were re-stimulated for 4 hr with 1
345 μM LCMV $GP_{61–80}$ or 0.1 μM GP_{33-41} peptide along with Brefeldin A (GolgiPlug Becton-Dickinson, 1
346 μl/mL) as published (41, 42). Cells were subsequently fixed by cell fixation/permeabilization solution
347 (Cytofix/Cytoperm, Becton-Dickinson) according to the manufacturer's protocol. For tetramer staining,
348 APC-conjugated $gp_{66–77}$:I-A^b and gp_{33-41}:H-$2D^b$ tetramers were provided by the NIH Tetramer Core
349 Facility (Emory Vaccine Center). Cell suspensions were incubated at 37°C for 3 hr in RPMI with the
350 tetramer followed by cell-surface staining. Tetramer fluorescence was normalized with isotype

351 tetramer (hCLIP:I-A^b) staining. Antibodies used for flow cytometry are presented in the Key Resources
352 Table.
353
354 **Bulk RNAseq**
355 CD4$^+$ T cells were purified from female Ly5.1 SMARTA and Ly5.1/5.2 SMARTA mice, and separately
356 transduced with pMIGR1-OCA-B or pMIGR1 (EV), respectively. On the following day, transduced
357 GFP$^+$ cells were sorted, 20,000 of each combined 1:1, and injected intravenously into 24 male
358 C57BL/6J male recipients. 24h later, each recipient mouse was injected intraperitoneally with 2x10^5
359 pfu LCMV. After eight days, the 24 mice were divided into six groups of four mice by combining four
360 spleens together. CD4$^+$ T cells were purified using a Miltenyi CD4 T cell isolation kit. Cells then were
361 stained with PerCP-Cy5.5 Ly5.1 and AF700 Ly5.2 antibodies. GFP$^+$Ly5.1$^+$Ly5.2$^+$ (EV) and
362 GFP$^+$Ly5.1$^+$ (OCA-B-expressing) cells were sorted by fluorescence-activated cell sorting (FACS) and
363 used for RNA purification (RNeasy Mini Kit, QIAGEN). RNA concentrations were determined using a
364 Quant-iT RNA assay kit and a Qubit fluorometer (ThermoFisher). Because limited RNA from EV-
365 transduced cells was obtained, the six EV samples were combined into three samples. Five OCA-B-
366 transduced samples (each comprising four mice) were submitted for RNAseq analysis. These showed
367 a high degree of concordance (not shown). Total RNA samples (200-500 ng) were hybridized with
368 Ribo-Zero Plus (Illumina) to deplete cytoplasmic and mitochondrial and ribosomal RNA from samples.
369 RNA sequencing libraries were prepared as described using the Stranded Total RNA Prep, Ligation
370 with Ribo-Zero Plus kit (Illumina) and IDT for Illumina RNA UD Indexes Set A, Ligation (Illumina).
371 Purified libraries were qualified on an Agilent Technologies 2200 TapeStation using a D1000
372 ScreenTape assay. The molarity of adapter-modified molecules was defined by qPCR using the Kapa
373 Biosystems Kapa Library Quant Kit. Individual libraries were normalized to 0.65 nM in preparation for
374 Illumina sequence analysis. Sequencing libraries were chemically denatured and applied to an
375 Illumina NovaSeq flow cell using the NovaSeq XP workflow (20043131). Following transfer of the flow
376 cell to an Illumina NovaSeq 6000 instrument, a 150 x 150 cycle paired-end sequence run was
377 performed using a NovaSeq 6000 S4 reagent Kit v1.5 (Illlumina).
378
379 **Bulk RNA-seq analysis**
380 Bulk RNA-seq analysis was performed as previously described (43). Briefly, Reads were aligned to
381 *Mm10* using STAR (v2.7.3a) and checked for quality using multiqc (v1.10). Between 12 and 14 million
382 pair-end reads were generated for each sample, with >98% of aligned reads mapping to the correct
383 strand and >93% of the reads uniquely aligned to the gene. Differentially expressed genes were
384 identified using DESeq2 version 1.24.0 (44) with a 5% FDR cutoff. Features with zero counts and 5 or
385 fewer reads in every sample were removed from the analysis. Genes increased by 1.4-fold or more or
386 decreased by 2-fold or more, and with adjusted $p<0.05$ were selected as differentially expressed (0.5

387 < log2FC < -1; padj ≤ 0.05). Figures were generated in R version 4.0.0 using functions from ggplots
388 libraries and pheatmap.
389
390 **Single-cell RNA-seq**
391 To profile gene expression at the single-cell level, splenic $GFP^+Ly5.1^+Ly5.2^+$ (EV-transduced) and
392 $GFP^+Ly5.1^+$ (OCA-B-transduced) SMARTA cells from four pooled mice per condition were isolated,
393 resuspended in PBS with 0.04% bovine serum albumin (ThermoFisher), and filtered through 40 μm
394 strainers. Viability and cell count were assessed using a Countess II (ThermoFisher). Equilibrium to
395 targeted cell recovery of 6,000 cells along with Gel Beads and reverse transcription reagents were
396 loaded to Chromium Single Cell A to form Gel-bead-in Emulsions (GEMs). Within individual GEMs,
397 cDNA generated from captured and barcoded mRNA was synthesized by reverse transcription at
398 53°C for 45 min. Samples were then heated to 85°C for 5 min. Single cell transcriptomes were
399 assessed using a 10X Genomics Chromium Single Cell Gene Expression instrument. Individual cells
400 were tagged with 16 bp barcodes, and specific transcripts with 10 bp Unique Molecular Identifiers
401 (UMIs) according to manufacturer instructions.
402
403 **Single-cell RNA-seq analysis**
404 Single cell transcriptome data were analyzed and clustered as described previously (43). Sequences
405 from the Chromium platform were de-multiplexed and aligned using CellRanger ver. 3.1.0 (10X
406 Genomics) with default parameters mm10-3.0.0. Clustering, filtering, variable gene selection and
407 dimensionality reduction were performed using Seurat ver.4.0.4 (45) according to the following
408 workflow: 1, Cells with <200 detected genes were excluded further analysis. 2, Cells with <5% UMIs
409 mapping to mitochondrial genes and *Cd44* expression >0 were retained for downstream analysis, as
410 SMARTA cells are uniformly responding to LCMV glycoprotein antigen at this time. 3, The UMI counts
411 per ten thousand were log-normalized for each cell using the natural logarithm. 4, Variable genes
412 (2000 features) were selected using the FindVariableFeatures function. 5, Common anchors between
413 the conditions were identified using FindIntegrationAnchors function that were further used to
414 integrate these sets. 6, Gene expression levels in the integrated set were scaled along each gene and
415 linear dimensional reduction was performed. The number of principal components was decided
416 through the assessment of statistical plots (JackStrawPlot and ElbowPlot). 7, Cells were clustered
417 using a shared nearest neighbor (SNN) modularity optimization-based clustering algorithm and
418 visualized using two-dimensional uniform manifold approximation and projection (UMAP). 8, One
419 cluster in each condition marked predominantly by mitochondrial genes (indicative of dying cells) was
420 excluded from the analysis. This resulted in 12,886 EV-transduced cells with 45,748 mean reads per
421 cell, and 2,595 median genes per cell. The total number of reads was 589,513,069, with 59.6%

422 mapping to exonic regions. Similarly, there were 11,709 OCA-B-transduced cells with 68,931 mean
423 reads per cell, and 2,668 median genes per cell. Total number of reads was 807,111,486, with 57.4%
424 mapping to exonic regions. Clusters were identified using manual interrogation of gene expression
425 enrichment for each population (Table S3), the ImmGene cluster identity predictor (Table S4, S5), and
426 PanglaoDB annotation terms. Clusters comprised of contaminating macrophages and neutrophils
427 were manually deleted.
428
429 **Memory progenitor isolation, normalization and transfer**
430 To assess contraction of the effector cells with different OCA-B levels, splenic $CD4^+$ T cells were
431 purified from 8 week-old female Ly5.1/5.2 homozygous knock-in reporter, SMARTA TCR transgenic
432 mice. 2×10^4 SMARTA cells were intravenously injected into 15 male Ly5.2/5.2 C57BL/6J recipients,
433 which were infected intraperitoneally 1 day later with 2×10^5 plaque-forming units of LCMV in 250 μL
434 phosphate-buffered saline. After 8 days, responding $Ly5.1^+5.2^+$ SMARTA T cells were sorted into
435 $mCherry^{hi}$ and $mCherry^{lo}$ populations. Cells were pooled and 8×10^5 $mCherry^{hi}$ and $mCherry^{lo}$ cells
436 were separately injected intravenously into 7 naïve age-matched 9 week-old male C57BL/6J
437 secondary recipients in the case of $mCherry^{lo}$ and 5 secondary recipients in the case of $mCherry^{hi}$.
438 After 8 additional days, mice were sacrificed and splenic $Ly5.1^+5.2^+$ SMARTA cells were counted by
439 flow cytometry. To assess proliferative responses to rechallenge, 15 similar virus-naïve secondary
440 recipients were rested for 43 days post-infection prior to isolation of $mCherry^{hi}$ and $mCherry^{lo}$
441 populations. 1.3×10^4 SMARTA cells were transferred into naïve recipients, which were infected with
442 LCMV one day later. 7 days post-infection, splenic $CD4^+Ly5.1^+5.2^+$ SMARTA cells were evaluated by
443 flow cytometry. Mice with poor infection/response (total splenocyte count $<6\times10^7$) were excluded from
444 the analysis.
445
446 **Quantification and statistical analysis**
447 Excel (Microsoft) and Prism (GraphPad) were used for statistics and graphing. Two-tailed Student T-
448 tests were used to ascribe statistical significance unless otherwise indicated. For all figures, *=*p*-
449 value≤0.05; **=*p*≤0.005; ***=p<0.001. All error bars denote ± standard error of the mean.

Acknowledgements: We thank M. Chandrasekharan for help with graphics. We thank J. Marvin and the University of Utah Health Sciences Center Flow Cytometry Core facility. We thank O. Allen, B. Dalley and the High-Throughput Genomics Core. MHC tetramers were provided by the NIH Tetramer Core Facility (Atlanta, GA). We thank R. Roeder for the mouse OCA-B cDNA and R. M. O'Connell for the pMIGR1 plasmid.

Funding: This work was supported by NIH grant R01AI100873 to DT.

Data and materials availability: All data are available in the main text or the supplementary materials. Materials used in the study are available to any researcher for purposes of reproducing or extending the findings. Bulk and single-cell RNA-seq data have been deposited at the Gene Expression Omnibus GEO) website (https://www.ncbi.nlm.nih.gov/geo/, GSE214310).

464 **Figure legends**

465 **Fig. 1.** Ectopic OCA-B expression enhances CD4+ T cell memory recall responses in vivo. (*A*)
466 Experimental schematic for OCA-B transduction and T cell mixed adoptive transfer. Ly5.1$^+$ SMARTA
467 cells were transduced with pMSCV-IRES-GFP (pMIGR1, EV) and Thy1.1$^+$ SMARTA cells were
468 transduced with pMIGR1 expressing mouse OCA-B (pMIGR1-OCA-B). The donors were age- and
469 sex-matched littermates. The next day following transduction, GFP$^+$ Ly5.1$^+$ SMARTA (EV) cells and
470 GFP$^+$ Thy1.1$^+$ SMARTA expressing OCA-B were sorted, combined 1:1, co-transferred into
471 Ly5.2$^+$/Thy1.2$^+$ C57BL6/J recipient mice, and infected with LCMV. Recipients were rechallenged with
472 Lm-gp61 on either day 52 or 110 post-LCMV infection, and in each case analyzed after 7 days. (*B*)
473 Lysates from NIH-3T3 cells transduced with either empty pMIGR1 (EV) or pMIGR1-OCA-B were
474 immunoblotted using antibodies against OCA-B. α-tubulin is shown as an internal loading standard.
475 (*C*) Flow cytometric analysis of Ly5.1$^+$ pMIGR1 EV-transduced and Thy1.1$^+$ pMIGR1-OCA-B-
476 transduced (OCA-B) SMARTA cells in the spleen and blood of a representative recipient mouse at
477 peak effector response (D8), peak memory recall response (52+7) and long-term memory recall
478 (D110+7). Cells were first gated based on CD44, CD4 and GFP positivity. (*D*) Mean relative
479 percentages of splenic and blood total EV- or pMIGR1-OCA-B-transduced (GFP$^+$) SMARTA cells
480 were plotted at D8, D52+7 and 110+7. Each datapoint represents an individual mouse harboring both
481 EV- and pMIGR1-OCA-B-transduced cells. 5, 7 and 10 mice were sacrificed at each timepoint to
482 obtain measurements from spleen. All mice were bled at D8, and remaining mice were bled at
483 subsequent timepoints. (*E*) Mean ratios of pMIGR1-OCA-B-transduced relative to EV-transduced
484 SMARTA cells (OCA-B/EV) are plotted. Splenic (top) and peripheral blood (bottom) SMARTA T cells
485 are shown at day 8 post-infection, or 7 days post-rechallenge with Lm-gp61 (52+7 or 110+7). (*F*) Flow
486 cytometry showing relative percentages of splenic GFP$^+$CD44^{hi} EV-transduced (blue) or pMIGR1-
487 OCAB-transduced (red) SMARTA cells expressing ICOS, PD-1, Ly6C or CD62L at day 8 post-
488 infection. Representative data showing the two populations of cells within a single mouse are shown
489 at day 8 post-infection. (*G*) Percent expression for ICOS, PD-1, CD62L and Ly6C was quantified from
490 four mice using splenic EV- and pMIGR1-OCAB-transduced GFP$^+$CD44^{hi} SMARTA cells at 8 days
491 post-infection. Four replicates were performed. For CD26L, the four datapoints are superimposed,
492 and for Ly6C two of the datapoints are superimposed. Individual mice are connected by lines.
493

494 **Fig. 2.** Gene expression changes associated with ectopic OCA-B expression in SMARTA transgenic
495 primary effector T cells. (*A*) Heatmap showing top up- and down-regulated genes. Genes with log2
496 fold-change >0.5 or <-1.0, and padj $\leq$ 0.05 are shown. Example genes are shown at right. Control
497 and OCA-B-transduced cells were purified from the same mice using magnetic isolation and FACS.
498 (*B*) Example genome tracks showing two up-regulated genes, *Socs2* and *Gadd45b*. *Pou2af1* (*Ocab*)

499 is shown as a positive control. (*C*) Top Epigenomic roadmap and Molecular function GO terms for the
500 set of OCA-B up- and down-regulated genes. (*D*) Top ChIP-X Enrichment Analysis (ChEA 2016)
501 factors potentially regulating the same set of genes up- and down-regulated by OCA-B ectopic
502 expression.
503
504 **Fig. 3.** Single-cell RNA-seq analysis of OCA-B-transduced vs. control SMARTA cells at 8 days post
505 LCMV infection. (*A*) UMAP projections of independently clustered EV-transduced (GFP^+) SMARTA
506 cells purified similar to Figs. 2 and 3, and subjected to scRNA-seq. Cluster identities were annotated
507 using a combination of gene expression enrichment (Table S3), cluster identity predictor ImmGen
508 identity scores (Table S4) and PanglaoDB annotation terms. Clusters 1 and 4 were associated with
509 memory formation. Top PanglaoDB annotation terms for cluster 4 are shown below. (*B*) Similar UMAP
510 projection using OCA-B-transduced cells purified from the same mice as in (A). Cluster identities were
511 annotated similarly to (A). Cluster 3 in OCA-B-transduced cells was most strongly associated with
512 memory formation. Top PanglaoDB annotation terms for cluster 3 are shown below.
513 (*C*) Feature plots highlighting expression of representative genes for the two UMAP projections in (A)
514 and (B). (*D*) UMAP projections of the the EV- and OCA-B-transduced single-cell RNA-seq datasets
515 clustered together. For each projection, the percentage of each cluster relative to the total number
516 cells in condition is shown. Cluster identities were annotated using a combination of gene expression
517 enrichment (Table S3), cluster identity predictor ImmGen identity scores (Table S5) and PanglaoDB
518 annotation terms. (*E*) Feature plots highlighting expression of representative genes for the combined
519 projections. (*F*) Violin plots depicting expression of six genes (*Il7r*, *Zeb2*, *Gadd45b*, *Foxo1*, *Tcf7* and
520 *Tox*) across each of the 10 clusters in EV-transduced cells (blue, left) and OCA-B-transduced cells
521 (red, right).
522
523 **Fig. 4.** mCherry expression in splenic T cell populations in specific pathogen-free homozygous OCA-
524 B-3×mCherry mice. (*A*) Mouse *Pou2af1* locus, targeting vector and the targeted *Pou2af1* locus. (*B*)
525 CD4 and CD8 expression are shown for an allelic series of example wild-type (+/+) and homozygous
526 (KI/KI) OCA-B knock-in reporter mice. (*C*) OCA-B homozygous reporter expression in splenic $CD4^+$ T
527 cell populations. (*D*) The same $CD4^+$ cells as in (C) were further stratified by CD62L and CD44 into
528 naïve, early activated, activated and central memory (Tcm) populations. $CD62L^{lo}CD44_{lo}$ cells are likely
529 recently activated cells that have down-regulated CD62L but not yet up-regulated CD44. (*E*) Similar
530 analysis as in (D) except for $CD8^+$ cells.
531
532 **Fig. 5.** $CD4^+$ T cells expressing high levels of OCA-B reporter activity preferentially form central
533 memory cells. (*A*) Schematic for assessing contraction of $mCherry^{hi}$ vs. $mCherry^{lo}$ SMARTA T cells
534 following LCMV infection. Congenically marked SMARTA T cells were isolated from donor mice,

535 transferred into naïve secondary recipients and infected with LCMV. At 8 days post-infection,
536 mCherry^{hi} and mCherry^{lo} populations were isolated by FACS. 8×10^5 SMARTA cells were transferred
537 into naïve recipients. After 8 days, splenic CD4$^+$Ly5.1$^+$5.2$^+$ SMARTA cells were evaluated by flow
538 cytometry. (*B*) Flow cytometric analysis of SMARTA donor T cells engrafted into naïve mice to monitor
539 rates of decline. Representative mice engrafted with mCherry^{lo} (left) or mCherry^{hi} (right) cells are
540 shown. (*C*) Quantification of averaged donor T cell numbers from mice engrafted with mCherry^{lo} or
541 mCherry^{hi} cells. N=7 for the mCherry^{lo} group and N=5 for the mCherry^{hi} group. (*D*) Similar analysis to
542 (C) except quantifying mean mCherry fluorescence intensity. (*E*) Schematic for assessing recall
543 responses of mCherry^{hi} vs. mCherry^{lo} SMARTA T cells following LCMV infection. Congenically
544 marked SMARTA T cells were isolated from donor mice, transferred into naïve secondary recipients
545 and infected with LCMV. However, mice were allowed to clear LCMV and form memory. After 43
546 days, mCherry^{hi} and mCherry^{lo} memory T cell populations were isolated by FACS. 1.3×10^4 SMARTA
547 cells were transferred into naïve recipients, which were infected with LCMV one day later. 7 days
548 post-infection, splenic CD4$^+$Ly5.1$^+$5.2$^+$ SMARTA cells were evaluated by flow cytometry. (*F*) Flow
549 cytometric analysis of SMARTA donor T cells 7 days post-rechallenge to monitor recall responses.
550 Representative mice engrafted with mCherry^{lo} (left) or mCherry^{hi} (right) cells are shown. (*G*)
551 Quantification of averaged donor T cell percentages and numbers from mice engrafted with mCherry^{lo}
552 or mCherry^{hi} cells. N=7 for the mCherry^{lo} group and N=5 for the mCherry^{hi} group. (*H*) Similar analysis
553 to (G) except quantifying mean mCherry fluorescence intensity. (*I*) Schematic for assessing mCherry
554 levels in SMARTA T at early timepoints following LCMV infection. 2×10^5 congenically marked
555 (CD45.1$^+$) SMARTA T cells were isolated from donor mice and transferred into naïve secondary
556 recipients. One day later mice were intraperitoneally infected with 2×10^5 PFU LCMV. Splenic T cells
557 were collected at 3 dpi. (*J*) Gated unfixed splenic CD4$^+$ T cells were assessed for the SMARTA
558 congenic marker Ly5.1 and mCherry (left), while fixed Ly5.1$^+$ (SMARTA) cells from the same mice
559 were used to assess CD25 and TCF1 (right). (*K*) CD25 and mCherry expression were assessed from
560 a representative animal. Left: distribution of SMARTA cell CD25 and mCherry expression in SMARTA
561 mice. Right: CD25 levels of gated mCherry^{hi} and mCherry^{lo} SMARTA cells displayed as a
562 concatenated histogram. (*L*) Quantification of averaged mCherry MFI in CD25^{hi} and CD25^{lo} cells (left),
563 and frequencies (center) and numbers (right) of CD25^{lo} cells in mCherry^{lo} or mCherry^{hi} cells SMARTA
564 T cells. N=6 independent recipient mice.

565 **References and Notes**

566 1. F. Sallusto, A. Lanzavecchia, K. Araki, R. Ahmed, From vaccines to memory and back.
567 *Immunity* **33**, 451-463 (2010).
568 2. S. V. Gearty *et al.*, An autoimmune stem-like CD8 T cell population drives type 1 diabetes.
569 *Nature* **602**, 156-161 (2022).
570 3. A. Schnell *et al.*, Stem-like intestinal Th17 cells give rise to pathogenic effector T cells during
571 autoimmunity. *Cell* **184**, 6281-6298 e6223 (2021).
572 4. P. C. Rosato *et al.*, Virus-specific memory T cells populate tumors and can be repurposed for
573 tumor immunotherapy. *Nat Commun* **10**, 567 (2019).
574 5. G. Cafri *et al.*, Memory T cells targeting oncogenic mutations detected in peripheral blood of
575 epithelial cancer patients. *Nat Commun* **10**, 449 (2019).
576 6. R. L. Rutishauser *et al.*, Transcriptional repressor Blimp-1 promotes CD8(+) T cell terminal
577 differentiation and represses the acquisition of central memory T cell properties. *Immunity* **31**,
578 296-308 (2009).
579 7. A. Kallies, A. Xin, G. T. Belz, S. L. Nutt, Blimp-1 transcription factor is required for the
580 differentiation of effector CD8(+) T cells and memory responses. *Immunity* **31**, 283-295 (2009).
581 8. H. M. Shin *et al.*, Epigenetic modifications induced by Blimp-1 Regulate CD8(+) T cell memory
582 progression during acute virus infection. *Immunity* **39**, 661-675 (2013).
583 9. L. Pace *et al.*, The epigenetic control of stemness in CD8(+) T cell fate commitment. *Science*
584 **359**, 177-186 (2018).
585 10. H. D. Marshall *et al.*, Differential expression of Ly6C and T-bet distinguish effector and
586 memory Th1 CD4(+) cell properties during viral infection. *Immunity* **35**, 633-646 (2011).
587 11. N. S. Joshi *et al.*, Inflammation directs memory precursor and short-lived effector CD8(+) T cell
588 fates via the graded expression of T-bet transcription factor. *Immunity* **27**, 281-295 (2007).
589 12. R. Hess Michelini, A. L. Doedens, A. W. Goldrath, S. M. Hedrick, Differentiation of CD8
590 memory T cells depends on Foxo1. *J Exp Med* **210**, 1189-1200 (2013).
591 13. R. R. Rao, Q. Li, M. R. Gubbels Bupp, P. A. Shrikant, Transcription factor Foxo1 represses T-
592 bet-mediated effector functions and promotes memory CD8(+) T cell differentiation. *Immunity*
593 **36**, 374-387 (2012).
594 14. M. Pepper, A. J. Pagan, B. Z. Igyarto, J. J. Taylor, M. K. Jenkins, Opposing signals from the
595 Bcl6 transcription factor and the interleukin-2 receptor generate T helper 1 central and effector
596 memory cells. *Immunity* **35**, 583-595 (2011).
597 15. H. Ichii *et al.*, Bcl6 is essential for the generation of long-term memory CD4+ T cells. *Int*
598 *Immunol* **19**, 427-433 (2007).
599 16. A. Banerjee *et al.*, Cutting edge: The transcription factor eomesodermin enables CD8+ T cells
600 to compete for the memory cell niche. *J Immunol* **185**, 4988-4992 (2010).
601 17. D. T. Utzschneider *et al.*, T Cell Factor 1-Expressing Memory-like CD8(+) T Cells Sustain the
602 Immune Response to Chronic Viral Infections. *Immunity* **45**, 415-427 (2016).
603 18. P. Sauter, P. Matthias, The B cell-specific coactivator OBF-1 (OCA-B, Bob-1) is inducible in T
604 cells and its expression is dispensable for IL-2 gene induction. *Immunobiology* **198**, 207-216
605 (1997).
606 19. S. Zwilling, A. Dieckmann, P. Pfisterer, P. Angel, T. Wirth, Inducible expression and
607 phosphorylation of coactivator BOB.1/OBF.1 in T cells. *Science* **277**, 221-225. (1997).
608 20. J. P. Snook, C. Kim, M. A. Williams, TCR signal strength controls the differentiation of CD4(+)
609 effector and memory T cells. *Sci Immunol* **3**, eaas9103 (2018).
610 21. S. Chevrier, T. Kratina, D. Emslie, A. Karnowski, L. M. Corcoran, Germinal center-
611 independent, IgM-mediated autoimmunity in sanroque mice lacking Obf1. *Immunol Cell Biol*
612 **92**, 12-19 (2014).
613 22. M. Nakamura *et al.*, Genome-wide association study identifies TNFSF15 and POU2AF1 as
614 susceptibility loci for primary biliary cirrhosis in the Japanese population. *Am J Hum Genet* **91**,
615 721-728 (2012).
616 23. M. Ban *et al.*, Linkage disequilibrium screening for multiple sclerosis implicates JAG1 and
617 POU2AF1 as susceptibility genes in Europeans. *J Neuroimmunol* **179**, 108-116 (2006).

24. H. Kim *et al.*, Targeting OCA-B/Pou2af1 blocks activated, autoreactive T cells in the pancreas and type-1 diabetes. *J Exp Med* **218**, e20200533 (2021).
25. H. Shen *et al.*, Recombinant Listeria monocytogenes as a live vaccine vehicle for the induction of protective anti-viral cell-mediated immunity. *Proc Natl Acad Sci U S A* **92**, 3987-3991 (1995).
26. A. Shakya *et al.*, Oct1 and OCA-B are selectively required for CD4 memory T cell function. *J Exp Med* **212**, 2115-2131 (2015).
27. A. Oxenius, M. F. Bachmann, R. M. Zinkernagel, H. Hengartner, Virus-specific MHC-class II-restricted TCR-transgenic mice: effects on humoral and cellular immune responses after viral infection. *Eur J Immunol* **28**, 390-400 (1998).
28. L. Liu *et al.*, Gadd45 beta and Gadd45 gamma are critical for regulating autoimmunity. *J Exp Med* **202**, 1341-1347 (2005).
29. P. Rodriguez-Jimenez *et al.*, Growth arrest and DNA damage-inducible proteins (GADD45) in psoriasis. *Sci Rep* **11**, 14579 (2021).
30. Y. Luo *et al.*, Suppression of collagen-induced arthritis in growth arrest and DNA damage-inducible protein 45beta-deficient mice. *Arthritis Rheum* **63**, 2949-2955 (2011).
31. S. Ju *et al.*, Gadd45b and Gadd45g are important for anti-tumor immune responses. *Eur J Immunol* **39**, 3010-3018 (2009).
32. A. Lachmann *et al.*, ChEA: transcription factor regulation inferred from integrating genome-wide ChIP-X experiments. *Bioinformatics* **26**, 2438-2444 (2010).
33. J. N. Blattman *et al.*, Estimating the precursor frequency of naive antigen-specific CD8 T cells. *J Exp Med* **195**, 657-664 (2002).
34. A. Crawford *et al.*, Molecular and transcriptional basis of CD4(+) T cell dysfunction during chronic infection. *Immunity* **40**, 289-302 (2014).
35. T. Samardzic, D. Marinkovic, P. J. Nielsen, L. Nitschke, T. Wirth, BOB.1/OBF.1 deficiency affects marginal-zone B-cell compartment. *Mol Cell Biol* **22**, 8320-8331 (2002).
36. R. Ahmed, A. Salmi, L. D. Butler, J. M. Chiller, M. B. Oldstone, Selection of genetic variants of lymphocytic choriomeningitis virus in spleens of persistently infected mice. Role in suppression of cytotoxic T lymphocyte response and viral persistence. *J Exp Med* **160**, 521-540 (1984).
37. C. Kim, D. C. Jay, M. A. Williams, Stability and function of secondary Th1 memory cells are dependent on the nature of the secondary stimulus. *J Immunol* **189**, 2348-2355 (2012).
38. D. M. Mitchell, E. V. Ravkov, M. A. Williams, Distinct roles for IL-2 and IL-15 in the differentiation and survival of CD8+ effector and memory T cells. *J Immunol* **184**, 6719-6730 (2010).
39. Y. Luo, R. G. Roeder, Cloning, functional characterization, and mechanism of action of the B-cell-specific transcriptional coactivator OCA-B. *Mol. Cell. Biol.* **15**, 4115-4124 (1995).
40. A. Shakya, J. Kang, J. Chumley, M. A. Williams, D. Tantin, Oct1 is a switchable, bipotential stabilizer of repressed and inducible transcriptional states. *J Biol Chem* **286**, 450-459 (2011).
41. K. Murali-Krishna *et al.*, Counting antigen-specific CD8 T cells: a reevaluation of bystander activation during viral infection. *Immunity* **8**, 177-187 (1998).
42. M. A. Williams, E. V. Ravkov, M. J. Bevan, Rapid culling of the CD4+ T cell repertoire in the transition from effector to memory. *Immunity* **28**, 533-545 (2008).
43. J. Perovanovic *et al.*, Oct1 cooperates with the Smad family of transcription factors to promote mesodermal lineage specification. *Sci. Signal.* **16**, eadd5750 (2023).
44. M. I. Love, W. Huber, S. Anders, Moderated estimation of fold change and dispersion for RNA-seq data with DESeq2. *Genome Biol* **15**, 550 (2014).
45. T. Stuart *et al.*, Comprehensive Integration of Single-Cell Data. *Cell* **177**, 1888-1902 e1821 (2019).

Sun et al. Figure 1

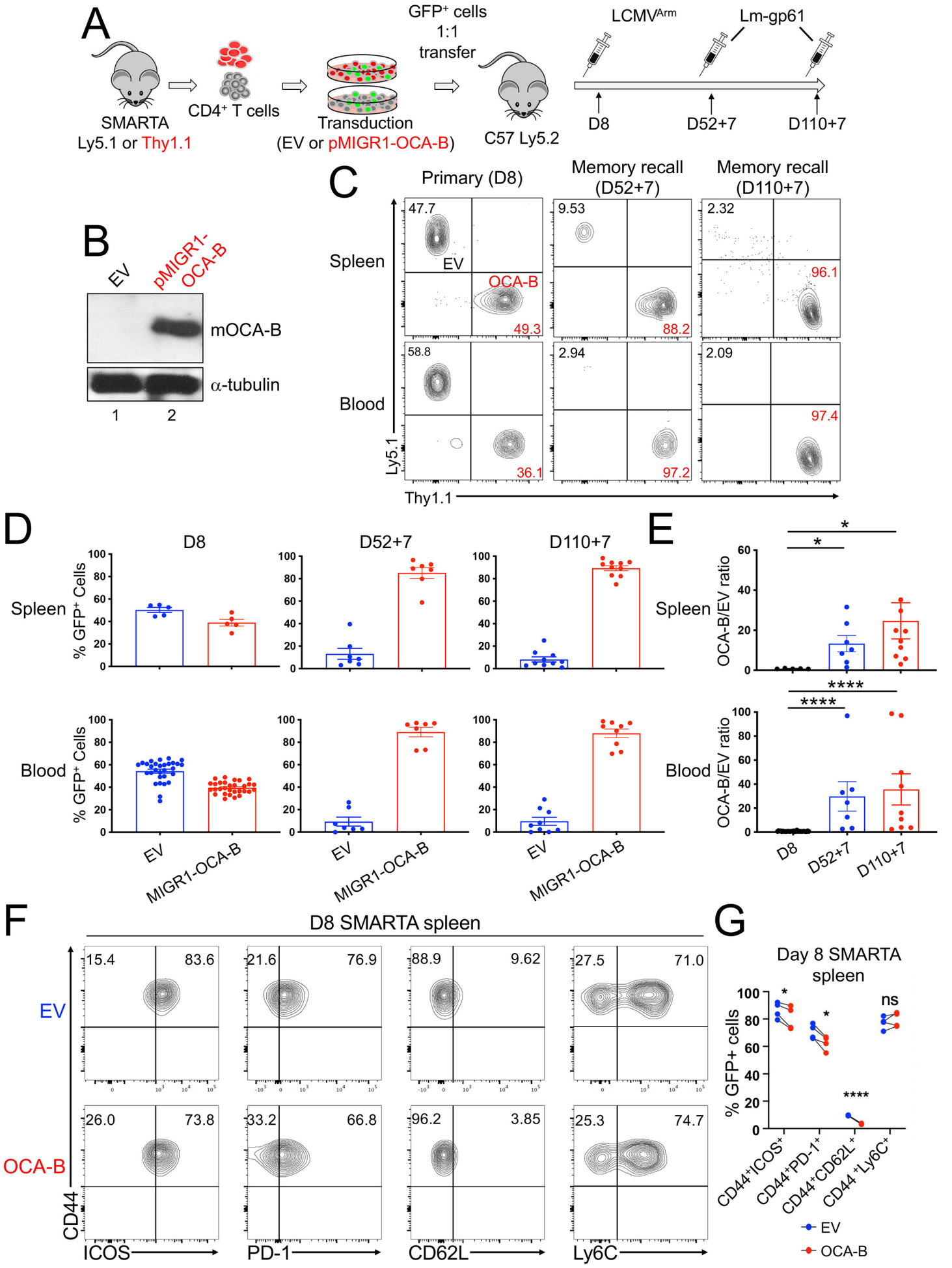

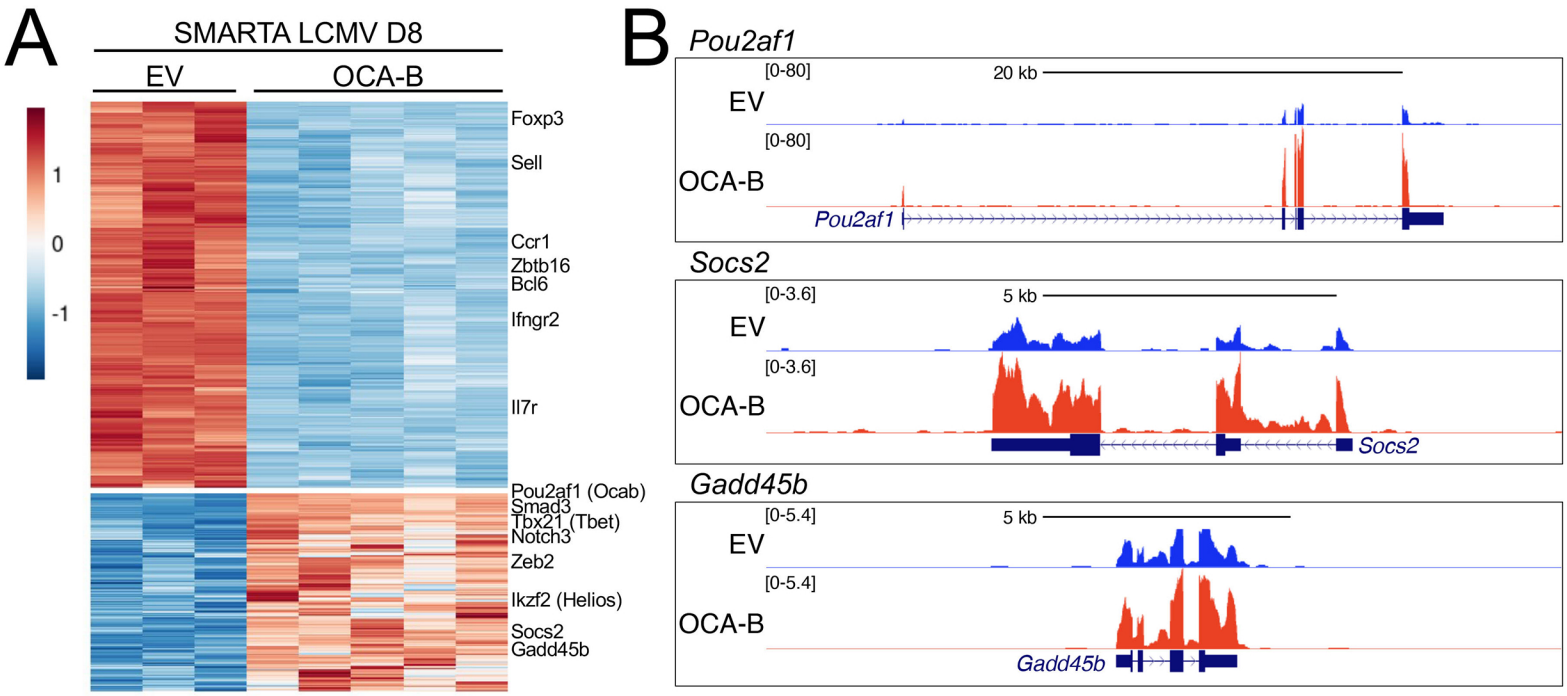

C

OCA-B upregulated genes

Epigenomic roadmap HM	*p*-value
H3K9me3 Breast vHMEC	0.048
Molecular function	***p*-value**
Toll-like receptor binding	0.006
Aspartic-type peptidase activity	0.007

OCA-B downregulated genes

Epigenomic roadmap HM	*p*-value
H3K27me3 CD4 Memory Primary Cells	1.45E-04
H3K27me3 CD8 Memory Primary Cells	9.30E-04
Molecular function	***p*-value**
Superoxide-generating NADPH oxidase activator activity	1.29E-09
Cytokine receptor activity	1.24E-06

D

OCA-B upregulated genes

ChEA 2016	*p*-value
Tp53	0.01936
Smc3	0.02544

OCA-B downregulated genes

ChEA 2016	*p*-value
IRF8	1.24E-20
SMRT	1.14E-15
MYB	1.73E-09
Nerf2	4.79E-09
NCOR	1.52E-08

Sun et al. Figure 3

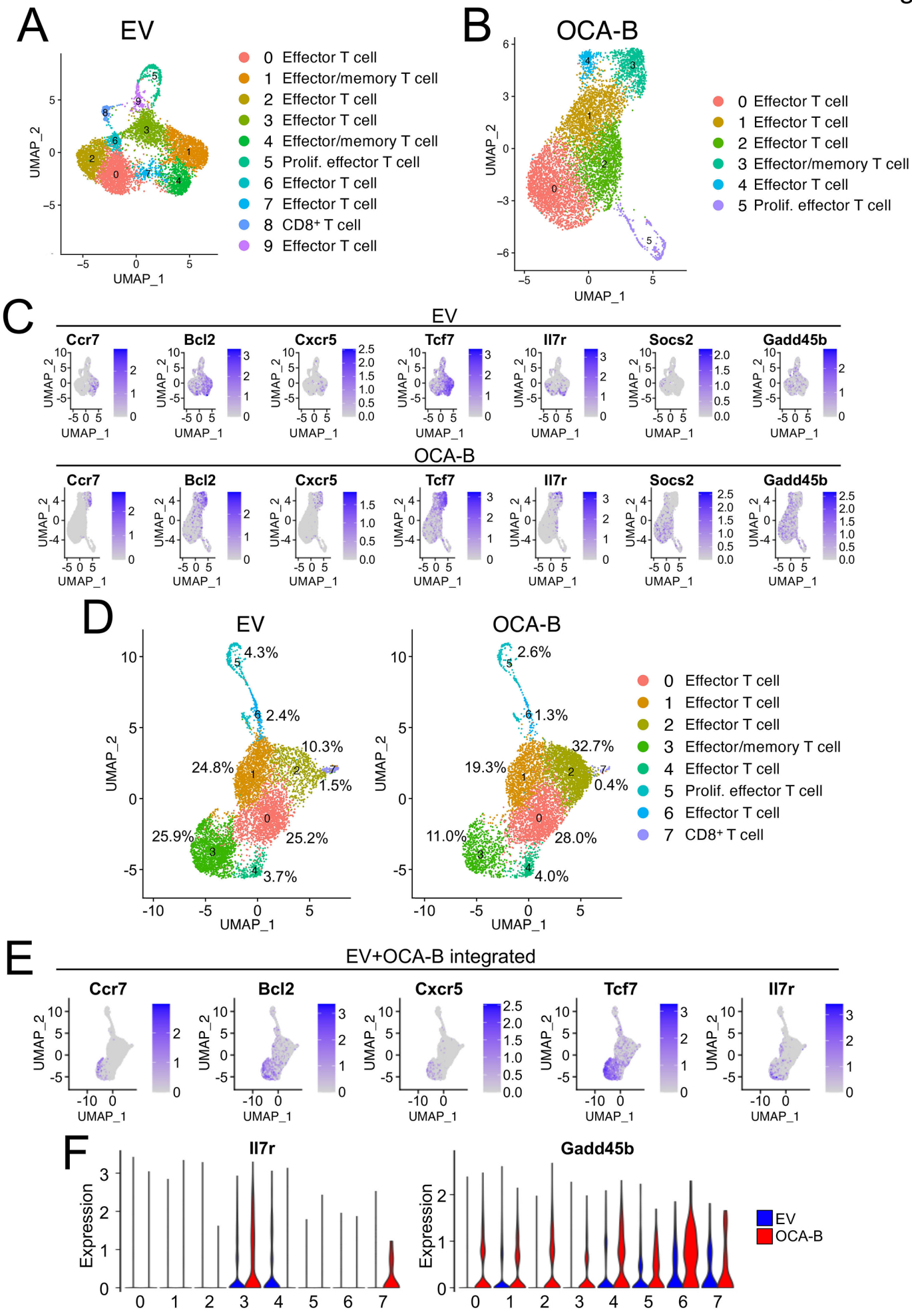

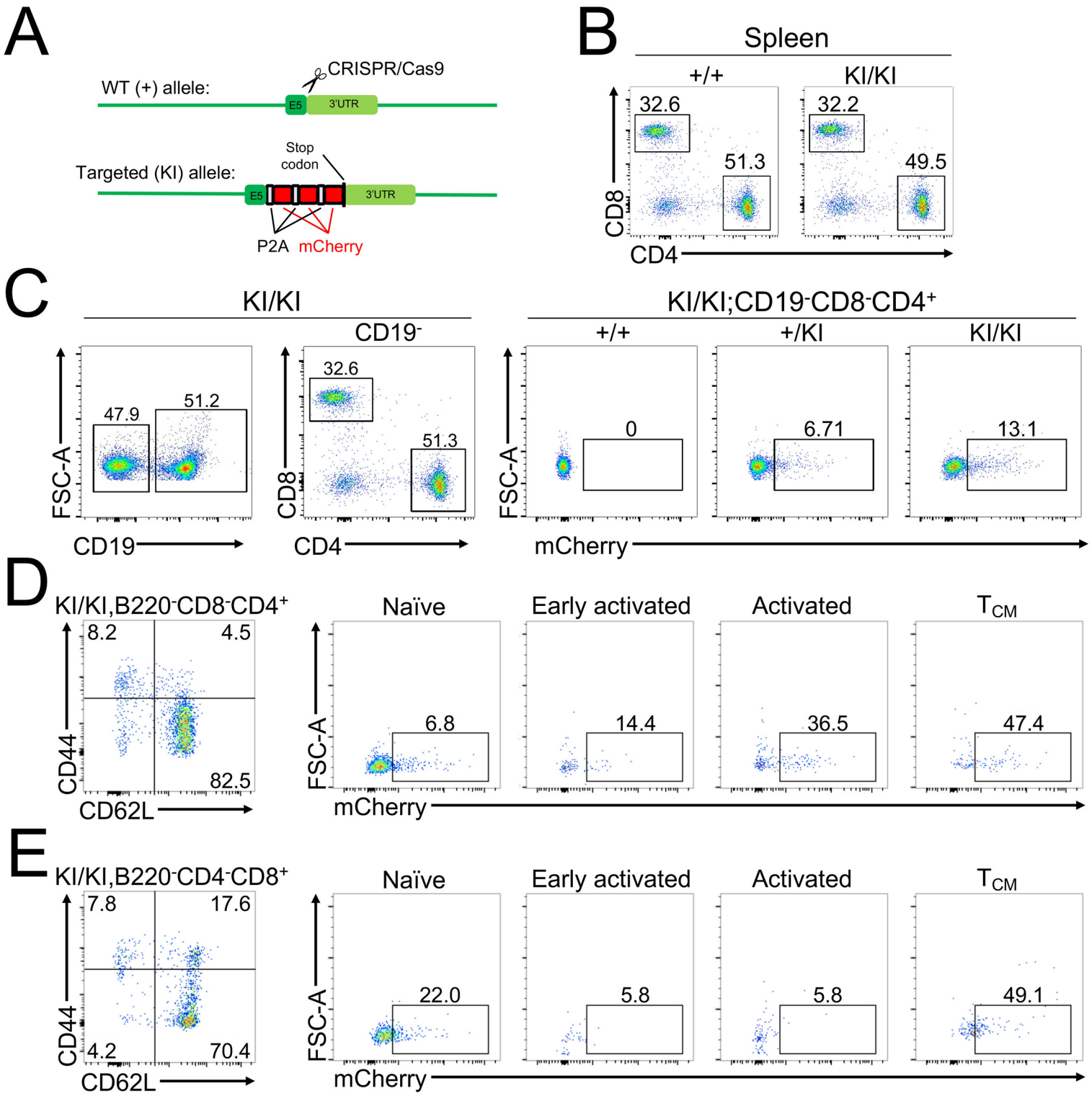
A
WT (+) allele:
CRISPR/Cas9
E5
3'UTR
Targeted (KI) allele:
Stop codon
E5
3'UTR
P2A
mCherry
B
Spleen
+/+
KI/KI
32.6
51.3
32.2
49.5
CD8
CD4
C
KI/KI
47.9
51.2
FSC-A
CD19
CD19-
32.6
51.3
CD8
CD4
KI/KI;CD19-CD8-CD4+
+/+
+/KI
KI/KI
0
6.71
13.1
FSC-A
mCherry
D
KI/KI,B220-CD8-CD4+
8.2
4.5
82.5
CD44
CD62L
Naïve
Early activated
Activated
TCM
6.8
14.4
36.5
47.4
FSC-A
mCherry
E
KI/KI,B220-CD4-CD8+
7.8
17.6
4.2
70.4
CD44
CD62L
Naïve
Early activated
Activated
TCM
22.0
5.8
5.8
49.1
FSC-A
mCherry
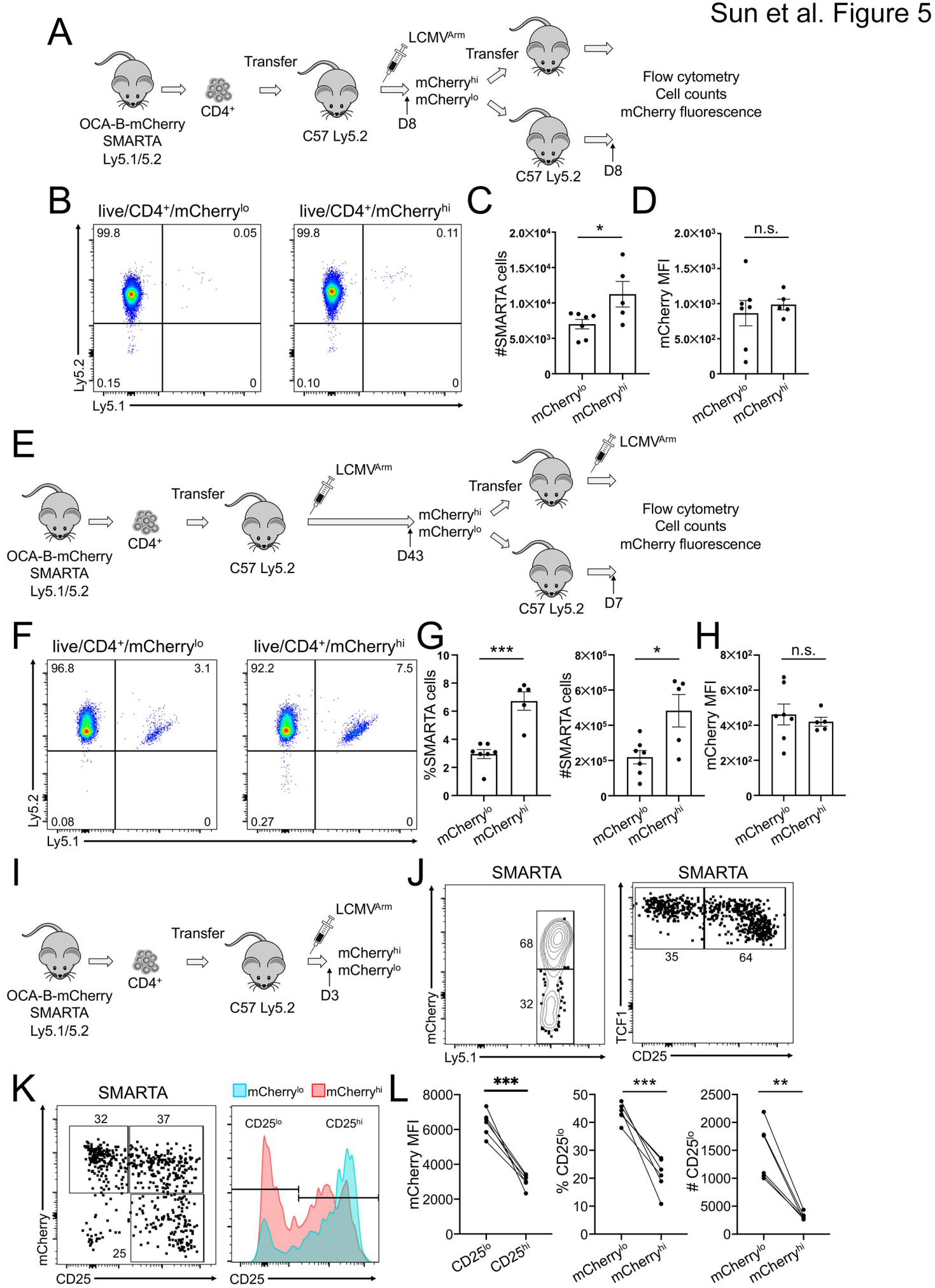
Sun et al. Figure 5